MOOR JOURNAL OF AGRICULTURAL RESEARCH
Journal homepage: https://iart.gov.ng/moorjournal/index.php/mjar/

Spatiotemporal analysis of land use dynamics and land surface temperature to detect environmental degradation in Ijebu-ode, Ogun State, Nigeria

[1]Adedeji, O. H., [2]Tobore, A. O., [3]Anoke, E. and [4]Tope-Ajayi, O. O.

[1]Department of Environmental Management and Toxicology, Federal University of Agriculture, Abeokuta, PMB 2240, Ogun State, Nigeria.

[2]Department of Soil Science and Land Management, Federal University of Agriculture, Abeokuta, PMB 2240, Ogun State, Nigeria.

[3]Land and Water Resources Management Programme, Institute of Agricultural Research and Training, Moor Plantation, Ibadan, Nigeria.

[4]Department of Geology, Federal University of Agriculture, Abeokuta, PMB 2240, Ogun State, Nigeria

Article Info

Article history:
Received: September 11, 2024
Revised: February 13, 2025
Accepted: February 18, 2025

Keywords:
land use/land cover
land surface temperature
Normalized difference vegetation index
Normalized difference built-up index

Abstract

In the face of escalating environmental challenges, the change in Land Use dynamics emerges as critical and persistent significant threat, profoundly impacting the stability of eco-biodiversity and food security challenges, especially in developing nations. This study examines the effect of land use/land cover changes (LULCCs) in Ijebu ode, Ogun State, Nigeria using Landsat Thematic Mapper (TM) and Landsat Operational Land Images (OLI) captured from United State Geological Survey repository. Herein, LULCCs maps for 2005, 2010, 2015, and 2020 including Normalized Difference Vegetation Index and Normalized Difference Built-up Index (NDBI) were examined to retrieve Land surface temperature of the area through Single-channel algorithm (SCA) method in order to detect the extent of degradation, contributing to the discourse on environmental sustainability. The results revealed the quantitative and qualitative environmental changes in the area, highlighting unprecedented built-up with an increase of 150.25 % while the non-built-up areas decreased by -56.77 % during the period of study. Undeniably, satellite remote-sensed data offers valuable tools to provide ecological information for urban sustainability. This study underscores the urgent attention from society, government, and stakeholders to manage population growth and balance human needs for a sustainable environment, thereby contributing to the broader goal of environmental sustainability.

Introduction

Numerous changes in land use and land cover have occurred during the past three decades as a result of the fast population growth and development of urbanization in both developed and developing regions of the world (Dijkstra *et al*., 2019; Adedeji *et al*., 2020; Zheng *et al*., 2021). Globally, urban areas have generally grown in size and quantity, which has resulted in the loss of natural and semi-natural lands (Chen *et al*., 2017). Approximately, 50% of the world's population, which is predicted to rise to more than 70% by the year 2050, would live in urban areas, according to estimations and projections from a number of organizations, including the United Nations (United Nations, 2018). In emerging nations around the world, notably in Africa and Asia, a large portion of the projected rapid urban population expansion is anticipated to take place in metropolitan and small cities (cities with a population of less than 0.5 million). However, it becomes expedient to highlight that urbanization is primarily tied to economic development as well as population increase among others. Interestingly, studies have shown that the city development model can have an impact on both the

Corresponding author: Tel: +2348108840248
Email address: toboreao@funaab.edu.ng, (A.O. Tobore)

environment and economic development (Wu *et al*., 2016; Ogunjobi *et al*., 2018; Li *et al*., 2020; Liu *et al*., 2022).

On one hand, urban population growth remains the driving force behind land use/and cover changes (LULCCs) which often resulted to urbanization due to the rapid growth of built-up areas, gradual to sudden increase in Impervious Surface Areas (ISAs), and a notable decrease in the area of agriculture, parks and gardens, water bodies, and wasteland (Wu *et al*., 2016; Ogunjobi *et al*., 2018; Zhang *et al*., 2022). These changes have significantly brought about a number of related global climate shocks and environmental changes in many regions of the world, including rising temperatures, declining urban air quality, and the Urban Heat Island (UHI) phenomenon (Chen *et al*., 2017; He *et al*., 2020; Yin *et al*., 2022). According to Oke (1987), an UHI is when the air and surface temperatures are higher in an urban area or metropolitan area than they are in a rural location. Although significant changes in the Urban Thermal Environment (UTE) and climate change variables, such as a decline in evapotranspiration and a differential land surface temperature (LST) between urban and suburban or nearby rural areas, have been brought on by rapid changes in urban LULCC patterns (Sun *et al*., 2012; Estoque *et al*., 2017; Rasul *et al*. 2017; Ranagalage *et al*., 2018; Chen *et al*., 2022). Besides, Land Surface Temperature (LST) have retained its potential ability and reliability to detect and monitor changes in Surface Urban Heat Island (SUHI) (Voogt and Oke, 2003; Li *et al*., 2013; Chen *et al*., 2017; Farid *et al*., 2022). Additionally, LST is sensitive to a variety of land surface characteristics especially regions with persistent expansion as a result of urbanization-related activities which often disrupt the ecosystem's ambient habitat for people and other living things (Voogt and Oke, 2003; Khandelwal *et al*., 2018; Kasim *et al*., 2020; Liu *et al*., 2021; Zhang *et al*., 2022). More importantly, LST have also been demonstrated to assess quick changes in surface temperature over time and space (Chen *et al*., 2017; Neog, 2021; Farid *et al*., 2022), thereby monitoring the eco-biodiversity changes and imbalances and thus mitigating on environmental health threats on food production (He *et al*., 2020). For these reasons, it is important to comprehend and enhance the urban thermal environment (Tiwari and Joshi, 2015; Liu *et al*., 2021) and having a solid understanding of LST is essential for many applications in cities and the environment because it offers adequate details on the temporal and spatial fluctuations of the surface equilibrium state (Orimoloye *et al*., 2018; Li *et al*., 2020; Zhang *et al*., 2022; Aigbokhan *et al*., 2023). Therefore, an attempt to assess qualitative and quantitative changes in Ijebu-Ode, Ogun state, Nigeria through NDBI, NDVI, and LST sandwiched with spatial LULCCs have been amply applied to assess urban degradation.

Methods and Materials

Description of study area

Ijebu-ode is a city in Ogun State, Nigeria's southwest. It is located between latitudes (6º42′N - 6º54′N) and Longitudes (3º55′E - 4º56′E), (Fig 1.) covering a total area of 8651.91hectares (86.52 sqkm), with the majority of the area being below 150 meters above sea level with annual rainfall ranging from 1575 mm to 2340 mm. The humid tropical climate of Ijebu-ode and its surrounding areas is characterized by alternate wet and dry season seasons. The parent materials of the studied area possessed basement rocks and sedimentary inclusion (Oke, 1987). However, rapid modification of the natural geomorphology and changes in land use cover of the region reveals its susceptibility to flash and pluvial flooding (Nkwunonwo *et al*. 2023). Consequently, with the increasing economic growth and socio-cultural activities, the region has been witnessing a significant expansion in industrialization and urbanization. The study area - Ijebu-ode was chosen due to its unprecedented and rapid urbanization over the last 20 years, which has been accompanied by rapid urban expansion and economic growth (Tiwari and Joshi, 2015). The city has encroached on other towns and villages in the surrounding area located approximately 110 km by road north-east of Lagos which highlight the country's commercial hub. Ijebu-ode is the second largest city in Ogun State, Nigeria, after the state capital, Abeokuta. According to the 2006 population census, the city has approximately 222,700 residents (NPC. 2006). According to the World Population Statistics by the Population HUB (2022), the current.

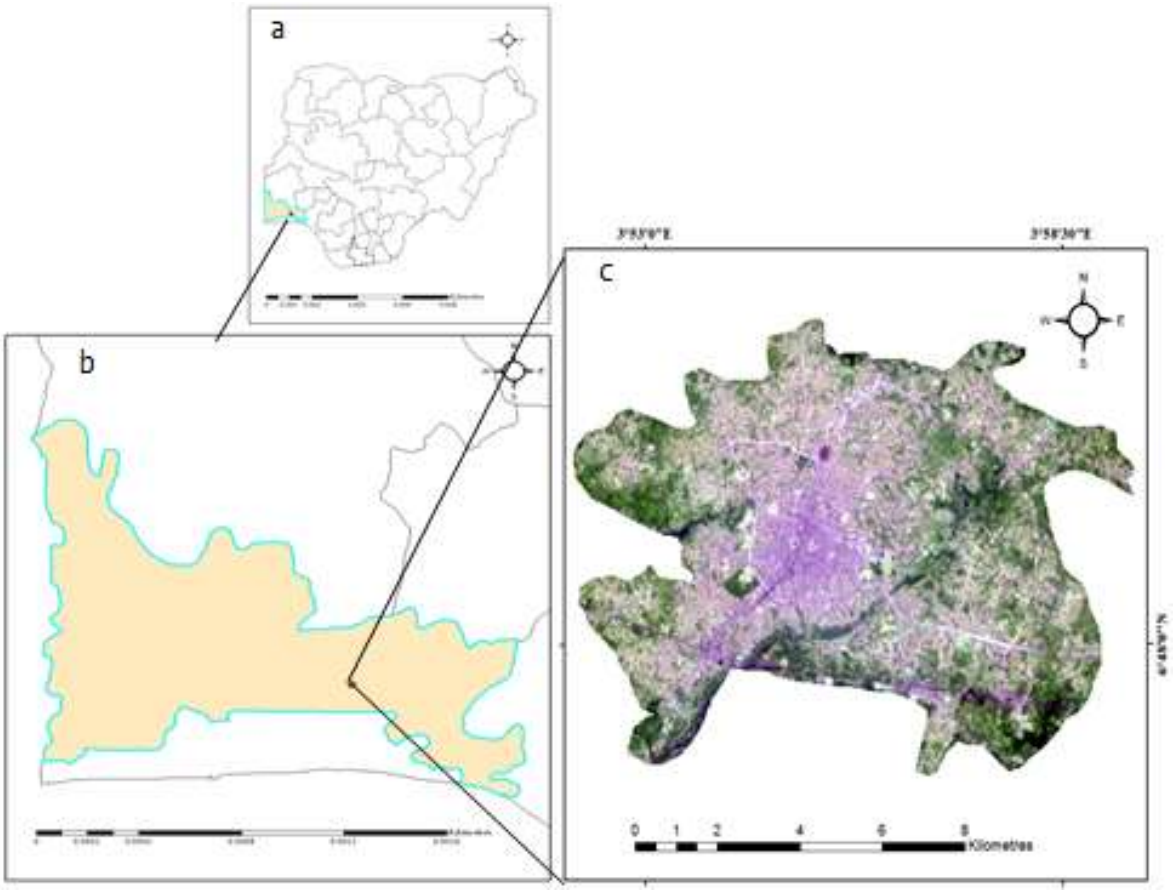

Fig. 1: Nigeria map within Ogun state (b) Generalized map of Ogun state enclosing the study area (c) Study area showing Google Earth image captured on 13 April 2020

population is estimated to be 403,836, making Ijebu-Ode one of 40 cities in Nigeria and ranking 25 in the Nigeria population

The methods

Landsat 5 Thematic Mapper (TM) and 8 Operational land images (OLI) acquired from 2005, 2010, 2015, and 2020 were prepared to explore the LULCCs of the area. The repositories of the United States Geological Survey (USGS) through 191 (path) and 55 (row) was utilized to download the satellite images to a resolution of 30 meters (m). The images were pre-referenced to World Geographic System (WGS) 84/UTM (Universal Transverse Mercator) Zone 31 North and masked through ArcGIS 10.5 software to avoid cloud patches (Orimoloye *et al*., 2018). After pre-processing, nearest-neighbour and second-order polynomial operations were applied to co-register the satellite images with a mean less than 0.5 pixels (Chen *et al*., 2017). Table 1 provides further detail on the specifications of the utilized Landsat images.

The processed Landsat were combined to create multiband-images, which was applied to produce the LULCC maps of the area. Firstly, the LULCCs maps were monitored based on the unsupervised using K-means algorithm and thereafter subjected to Maximum likelihood supervised classification algorithm through IDRISI Selva software. The essence of these operations is due to the large extent of the studied area in order to obtain high accuracy and potential ability to classify satellite imagery into different land use cover classes (Tobore *et al*. 2024). Therefore, we identified four classes namely Builtup: (Residential, commercial, and industrial), Waterbodies: (Rivers and streams), Vegetation: (Dense, and sparse forest); and bareground (impervious surface). The terrestrial reality control sampling points combined with Google Earth images were set at a random to check the accuracy of the LULCC maps.

Table 1: Descriptions of landsat resources used in Ijebu-Ode city

S/No.	Sensor	Date of Acquisition	Path/Row	Band combination used	Resolution (m)	Format	Source
1	Landsat 5 TM	December 18, 2005	191/055	1,2,3,4,5, 6 and 7	30 meters	GeoTIFF	USGS
2	Landsat 7 TM	January 01, 2010	191/055	1,2,3,4,5, 6 and 7	30 meters	GeoTIFF	USGS
3	Landsat8 OLI_TIR	January 06, 2015	191/055	1,2,3,4,5, 6 and 7	30 meters	GeoTIFF	USGS
4	Landsat8 OLI_TIR	January 04, 2020	191/055	2,3,4,5, 6,7, 10 and 11	30 meters	GeoTIFF	USGS

Satellite based environmental degradation

Normalized difference vegetation index (NDVI)

Although there are several vegetation indices, each with its own set of strengths and weaknesses (Loranty *et al*., 2018; Huang *et al*., 2021), the Normalized difference vegetation index (NDVI) is the most commonly used index for vegetation assessment. It is used to distinguish healthier vegetation, which reproduces exceptionally well in the near portion of UV EMR (full meaning). NDVI is based on the fact that vegetation absorbs strongly in the red band and reflects strongly in the near-infrared band (Wu *et al*., 2016). The NDVI scale runs from -1 to 1. The values are positive for vegetation such as crops, shrubs, grasses, and forests and near zero or negative for non-vegetated areas such as built-up areas and concrete surfaces, rocks, and sand (Huang *et al*., 2021; Zheng *et al*., 2021). It is calculated using equation (1) for Landsat-5 TM and Landsat-8 OLI respectively:

$$NDVI = \frac{\rho NIR - \rho RED}{\rho NIR + \rho RED} \qquad 1$$

where NDVI = normalized difference vegetation index, ρNIR is the surface reflectance of band 4, and ρRed is the surface reflectance of band 3 in Landsat 5 and 7, and band 5 and band 4 in Landsat 8).

Normalized difference built up index (NDBI)

The normalized difference built up index (NDBI) was used to distinguish between built up and unbuilt pixels in the study area, and it was validated by land use/land cover maps generated over three different time periods (2005, 2010, 2015, and 2020). NDBI was created by using mid-infrared (MIR) and near-infrared (NIR) bands to differentiate built-up pixels based on pixel radiance values (Liu *et al*., 2021). Built-up lands have higher reflectance in the MIR wavelength range (1.55~1.75μm) than in the NIR wavelength range (0.76 ~ 0.90μm) when compared to other land use / land cover surfaces. The NDBI values were calculated using the method described by Zha *et al*. (2003) in equation (2):

$$NDBI = \frac{MIR - NIR}{MIR + NIR} \qquad 2$$

where NDBI is the dimensionless normalized difference build-up index, *MIR* is Band 5 in Landsat TM, and Band 6 in Landsat 8. In Landsat TM, *NIR* is

Band 4 and in Landsat 8, it is Band 5. NDBI values ranging from 0 to (positive) +1 indicate built-up land, while values closer to 1 indicate densely built-up land (Zha *et al*., 2003; He *et al*., 2020; Choudhury *et al*., 2019; Zheng *et al*., 2021). It should be noted that the reflectance of built-up areas is higher in the *MIR* wavelength range (1.55 ~ 1.75μm) than in the *NIR* wavelength range (0.76 ~ 0.90μm). In general, a higher proportion of built-up and bare soil is indicated by a positive value. Other land uses were represented by negative values.

Impervious surface area (ISA)

The impervious surface area (ISA) for the study area was calculated in ArcGIS using Rasul *et al*. (2017). The term "impervious surface areas" refers to urban built-up areas and the man-made coverings and constructions (Rasul *et al*., 2017). ISA is calculated from the following equation (3):

$$ISA = (1 - F)_{dev} \quad 3$$

where $F = Pv$, while *dev* indicates that the quantity is only defined for urban developed regions.

Pv is calculated using the equation (4):

$$Pv \equiv \left(\frac{NDVI - NDVI_{\min}}{NDVI_{\max} - NDVI_{\min}} \right)^2 \quad 4$$

where NDVI is the normalized difference vegetation index. NDVImin and NDVImax are the minimum and maximum values of the NDVI, respectively.

LST Retrieval from Landsat-5 and Landsat-8

Through the development of various algorithms, there have been significant improvements in the estimation of LST from satellite TIR (Thermal Infrared) sensors measurements over the last several decades. The Mono Window Algorithm (MWA), Single Channel Algorithm (SCA), Split Window Algorithm (SWA), Radiative Transfer Equation (RTE), and NDVI-based LSE (Land surface emissivity) Algorithm have all been used to estimate LST from Landsat data (Sobrino *et al*., 2008). The NDVI-based LSE method used in this study is the most commonly used method in LST retrieval because it is simple to compute and produces good results (Sobrino *et al*., 2008). The current study used an NDVI-based LSE method to estimate LST.

Retrieval of Satellite Brightness Temperature (BT) from the Landsat-5 Images

Satellite imagery, according to Li *et al*. (2015), measures the radiance of surface features modified by the atmosphere. The LST for the various study periods were obtained using single-channel (SC) algorithms based on known LSE. LST was extracted from Landsat 5 TM images' thermal data from sensors with a single TIR channel. To retrieve the LST more accurately, radiometric calibration, atmospheric, and emissivity corrections were performed (Qin *et al*., 2001). The brightness temperature was extracted from Landsat-5 TM (Thematic Mapper) images in two steps. The digital numbers (DNs) of band 6 were first converted into radiation luminance (RTM6) using the following equations (5, 6, and 7):

$$R_{TM6} = \frac{V}{255}(R_{\max} - R_{\min}) + R_{\min} \quad 5$$

where V represents the DN of band 6, and

$$R_{\max} = 1.896(mW * cm^{-2} * sr^{-1}), \quad 6$$

$$R_{\min} = 0.1534(mW * cm^{-2} * sr^{-1}) \quad 7$$

Radiation luminance was then transformed into satellite Brightness Temperature (BT) in Celsius (°C), using equation (8):

$$BT = \frac{K1}{(\ln(K2/R_{TM6}/b) + 1)} - 273.5 \quad 8$$

where K1 = 1260.56 and K2 = 607.66 ($mW * cm^{-2} * sr^{-1}$ μm^{-1}), which are prelaunch calibration constants under an assumption of unity emissivity; and *b* represents the effective spectral range when the sensor's response is considerably higher than 50%, *b* = 1.239 (μm). Furthermore, retrieval of satellite Brightness Temperature (BT) from the Landsat-8 Image assisted to produce the normalized difference vegetation index (NDVI) to estimate LST. The first step is to use the formula in equation (1) to calculate the NDVI for the study periods. The next step is to convert the DN of the thermal infrared band to spectral radiance (L) or TOA (Top of Atmospheric) spectral radiance using equation (9) from the Landsat 8 user's handbook (USGS, 2016):

$$L_\lambda = M_L * Q_{CAL} + A_L \quad 9$$

where: L_λ is the at-sensor spectral radiance in watts/ ($m^2 * ster * \mu m$),

Qcal are the quantized and calibrated standard product pixel values,

ML is the band-specific multiplicative rescaling factor from the metadata, and
AL is the band-specific additive rescaling factor

After the band radiance is then converted into BT in Celsius using equation (10):

$$BT = \frac{K2}{Ln\left(\left(K1/L_{\lambda}\right)+1\right)} - 273.15 \qquad 10$$

where BT denotes the satellite brightness temperature in Celsius and K1 and K2 denote thermal conversion from metadata. Landsat 8 bands 10 was considered. K2 = 1321.08 and K1 = 774.89 ($mW*cm^{-2} * sr^{-1} \mu m^{-1}$) for Band 10, while K2 = 1201.14 and K1 = 480.89 ($mW*cm^{-2} * sr^{-1} \mu m^{-1}$). These are the prelaunch calibration constants assuming unity emissivity.

Land surface emissivity (ε) values were obtained using equation (11) (Sobrino *et al*., 2008)

$$\varepsilon = m * Pv + n \qquad 11$$

In this study, we used $m = 0.004$ and $n = 0.986$. Correction of emissivity was done before the retrieval of the LST to remove errors in surface temperature. Finally, the LSTs were extracted for the study period using equation (12):

$$LST = \frac{BT}{\left(1+\left(\lambda * BT / p\right) * In\left(\varepsilon\right)\right)} \qquad 12$$

where LST is Celsius, BT is the at sensor brightness temperature in Celsius, λ (11.5 μm) is the wavelength of the emitted radiance: $\rho = h*c/\sigma = 1.438*10^{-2}$ mK, σ is the Stefan–Boltzmann constant, h is Planck's constant, c is the velocity of light, and ε is the land surface emissivity (LSE).

Statistical Analysis of Landscape Indices (LST, NDVI and NDBI)

Correlations between calculated LST, NDVI, and NDBI were calculated using 2500 randomly generated points in ArcGIS using the random point's tool. After that, the multi values to point tool in ArcGIS was used to extract values from the LST, NDVI, and NDBI layers for the study periods 2005, 2010, 2015, and 2020. Finally, scatterplots for the relationships were created. A stepwise workflow has been described in Fig. 2.

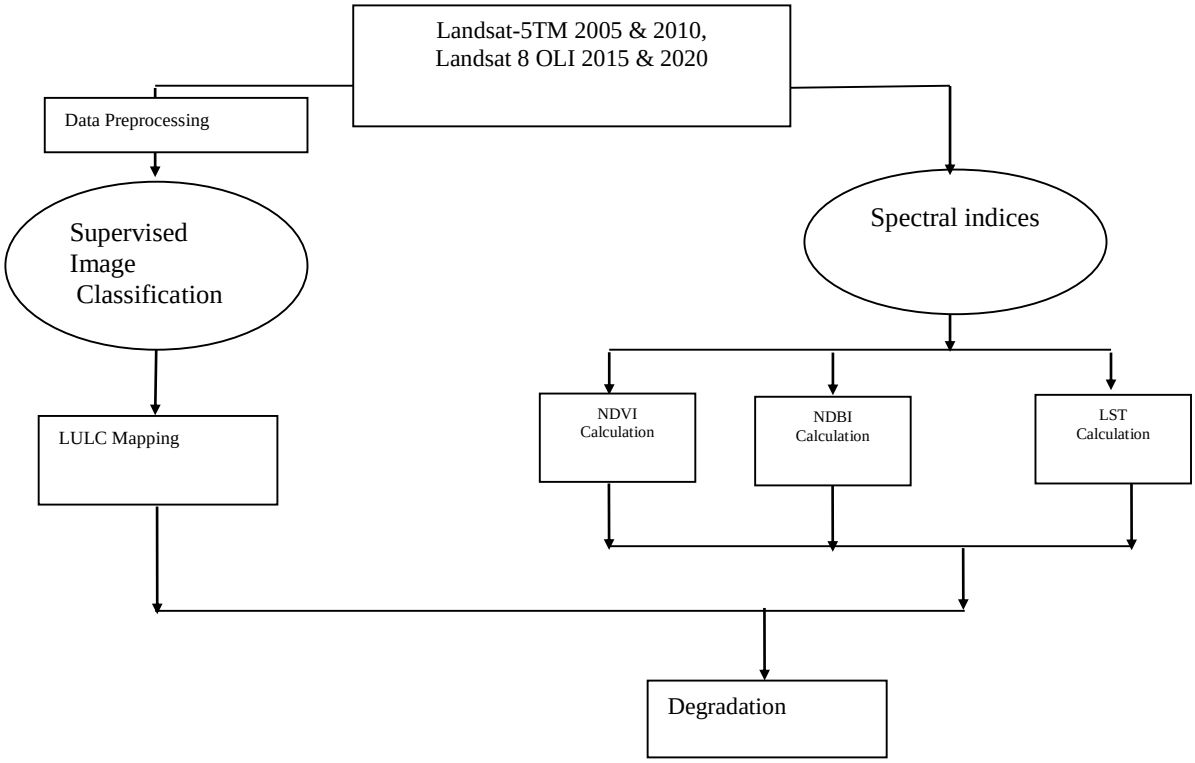

Fig. 2: Flowchart of the methodology for the current study

Results

Understanding the science of LULCC change is essential for mitigating consequences of human and environmental interactions that reshape the earth surface (Tobore *et al.*, 2024). Table 2 illustrates the relative distribution of land use/land cover classes in Ijebu-ode in 2005, 2010, 2015, and 2020. In this study, four land use/land cover categories were identified using Maximum likelihood classification (MLC): built-up area, bareground, vegetation, and water body. Fig. 3 depicted the classified images of the study area during the reference period. The built-up area grew as a result of rising population and infrastructure development in the studied area. Bareground experienced both positive and negative changes during the study under review.

During the study period, the proportion of bareground was 592.83 ha (6.85%), 254.38 ha (2.94%), 149.81 ha (1.73%), and 259.87 ha (3.00%), respectively (Fig. 4). These substantial changes could be attributed to activities such as farming, deforestation, indiscriminate bush burning, and the rapid urbanization of built-up areas. Over the last 15 years, there has been a significant change in land use/land cover in the study area. In 2005, vegetation had a 64.23% share of the land cover, followed by built-up areas (about 27.44%), bare ground (6.85%), and water bodies (1.48%). The vegetation and agricultural lands were observed to have a significant reduction in area covered from 5557 hectares in 2005 to 2307.8 hectares by 2020. During the same time period, built-up area increased by 150.25%, from 2374.30 hectares to 5941.62 hectares. Table 1 shows the changes in area under different land use/land cover classes in Ijebu-ode during the study period. The Normalized Difference Vegetation Index (NDVI), which is the sum of vegetation and quality at the earth's surface, is shown for the study area (Fig. 4). NDVI values range from -1 to +1, with higher NDVI values indicating richer and healthier vegetative cover. The values are negative for bodies of water and close to zero for bare surfaces, rocks, sands, or concrete surfaces. In 2005, 2010, 2015, and 2020, the distribution range and corresponding mean value of the NDVI ranged from -0.10 to 0.26 with a mean of 0.12, -0.126 to 0.884 with a mean of 0.526, and -0.164 to 0.854 with a mean of 0.473, respectively. The changes in built-up areas in the study area were assessed by creating NDBI maps of study periods. The results of the NDBI and NDVI were used to compute the ISA or the built-up areas as shown in Figs. 5 and 6. The minimum and maximum NDBI values were -0.080 and 0.393 in 2005, 0.050 and 0.487 in 2010, -0.196 and 0.072 in 2015, and -0.257 and 0.167 in 2020.

The spatial distribution of LSTs in the study area was calculated using the Landsat thermal band for the study periods 2005, 2010, 2010, and 2020 (Fig. 7). The areas with the highest LST are shown in dark red, while the areas with the lowest LST are shown in blue. The study found that the LST pattern varies significantly throughout the study period. The spatial distribution clearly showed that built-up areas and baregrounds had higher LST than vegetation and water bodies. The temperature ranged from 19.73 ºC to 26.25 ºC in 2005, with a mean LST of 22.17ºC. Although the spatial pattern of LST in the study area did not change significantly between 2015 and 2020, there was a general increase in the overall mean temperature as the rate of urbanization increased, with the mean LST for 2020 being 26.62 ºC, representing a 4.60 ºC increase and the temperature ranging between 23.08 ºC and 30.56 ºC. LSTs were ranked in the following order: built-up > bareground > vegetation > water bodies.

Table 2: land use/land cover classes of Ijebu-ode in 2005, 2010, 2015 and 2020

LULC	2005		2010		2015		2020	
	Ha	%	Ha	%	Ha	%	Ha	%
Built-up	2374.30	27.44	3088.35	35.68	4758.65	54.97	5941.62	68.65
Vegetation	5557.08	64.23	4725.27	54.58	3629.78	41.93	2307.78	26.66
Bareground	592.83	6.85	254.38	2.94	149.81	1.73	259.87	3.00
Water bodies	127.70	1.48	588.90	6.80	118.87	1.37	146.29	1.69
Total	8651.91	100.00	8656.90	100.00	8657.11	100.00	8655.56	100.00

Ha = Hectare

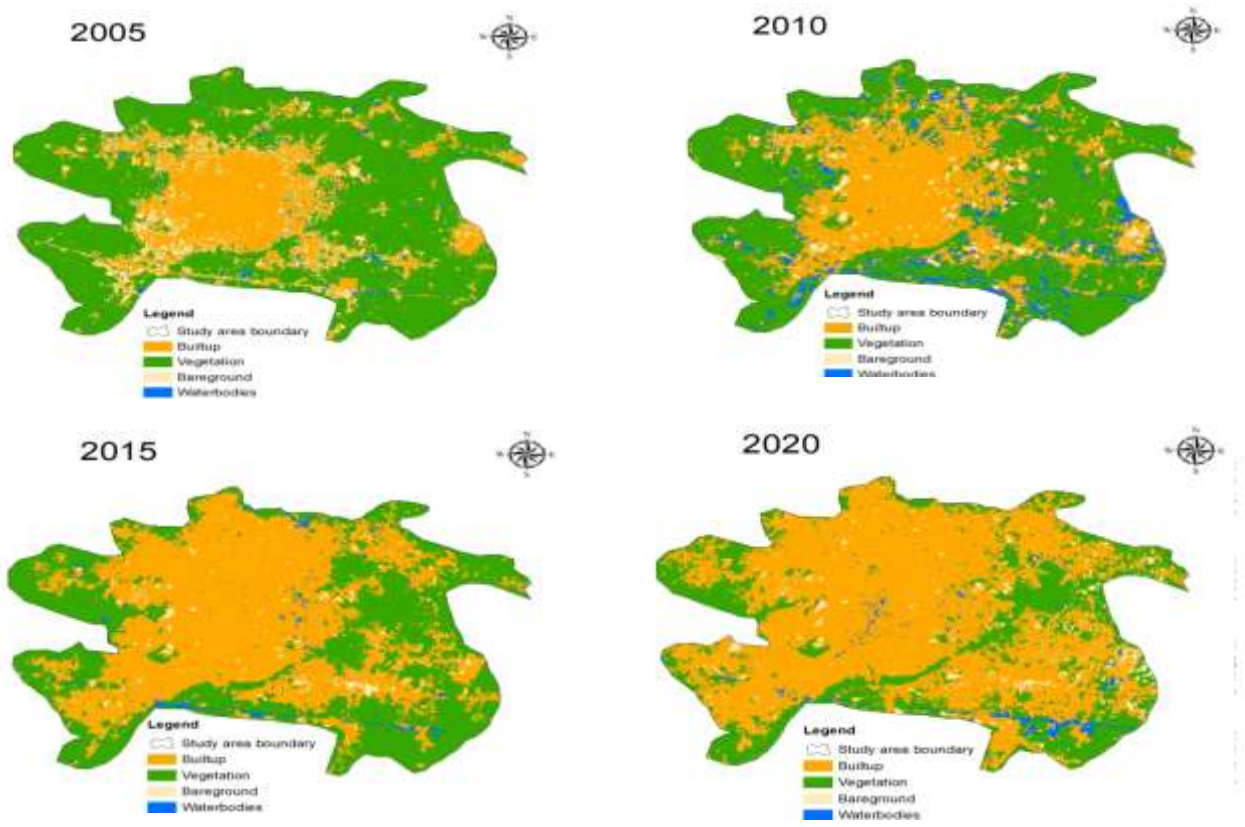

Fig. 3: Land use/Land cover maps of Ijebu-ode on December 18 2005, January 01 2010, January 06 2015 and January 04 2020

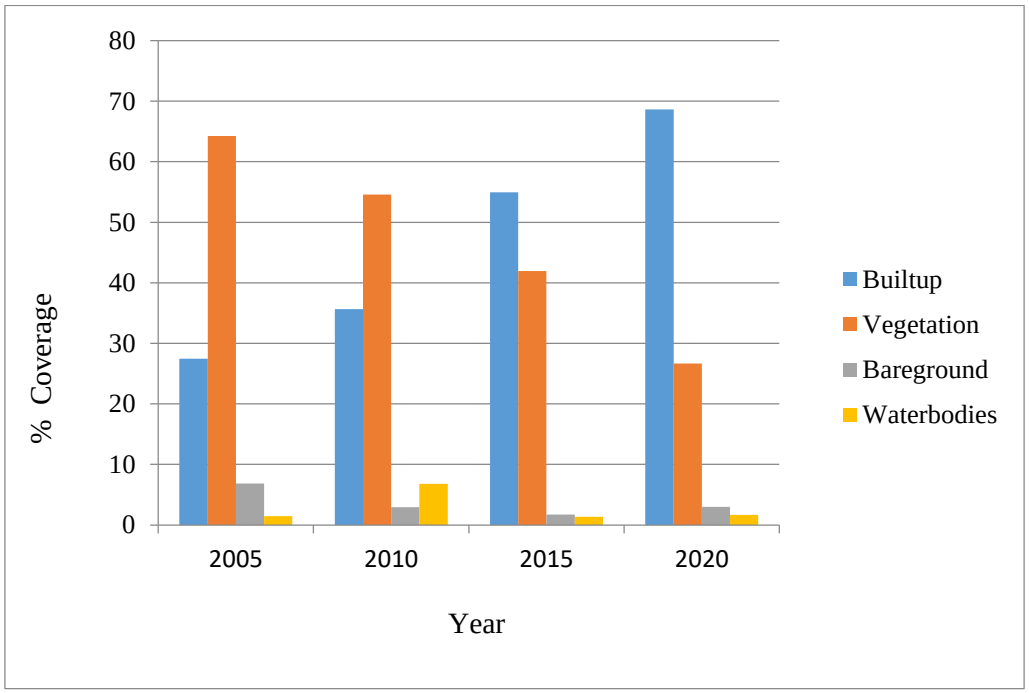

Fig. 4: Percentages of land cover types in different years in Ijebu-ode

Table 3: Changes in area under different LULCC classes in Ijebu-ode (2005-2020)

Land use/land cover classes	Area in Hectares				Rate of change			
	2005	2010	2015	2020	2005-2010	2010-2015	2015-2020	2005-2020
Built-up	2374.3	3088.35	4758.65	5941.62	30.07	54.08	24.86	150.25
Vegetation	5557.08	4725.27	3629.78	2307.78	-14.97	-23.18	-36.42	-58.47
Bareground	592.83	254.38	149.81	259.87	-57.09	-41.11	73.47	-56.17
Water bodies	127.7	588.9	118.87	146.29	361.16	-79.82	23.07	14.58

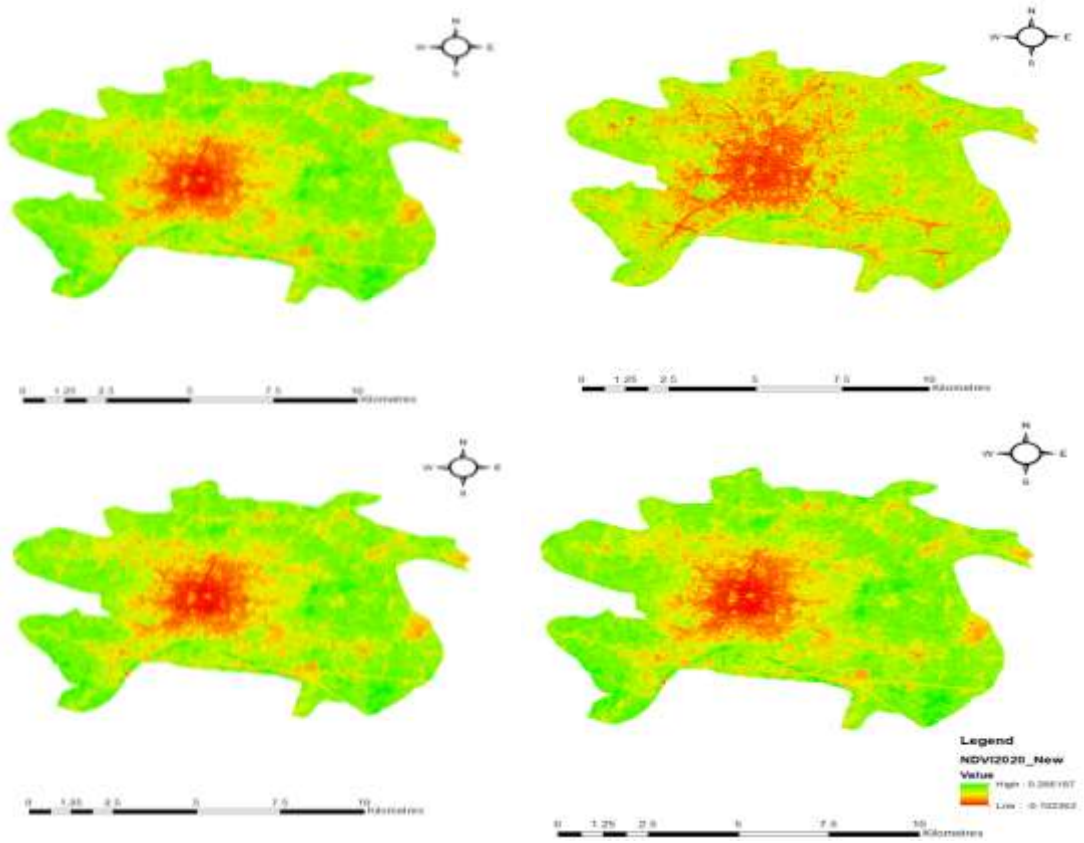

Fig. 5: NDVI maps of Ijebu-ode on December 18 2005, January 01 2010, January 06 2015 and January 04 2020

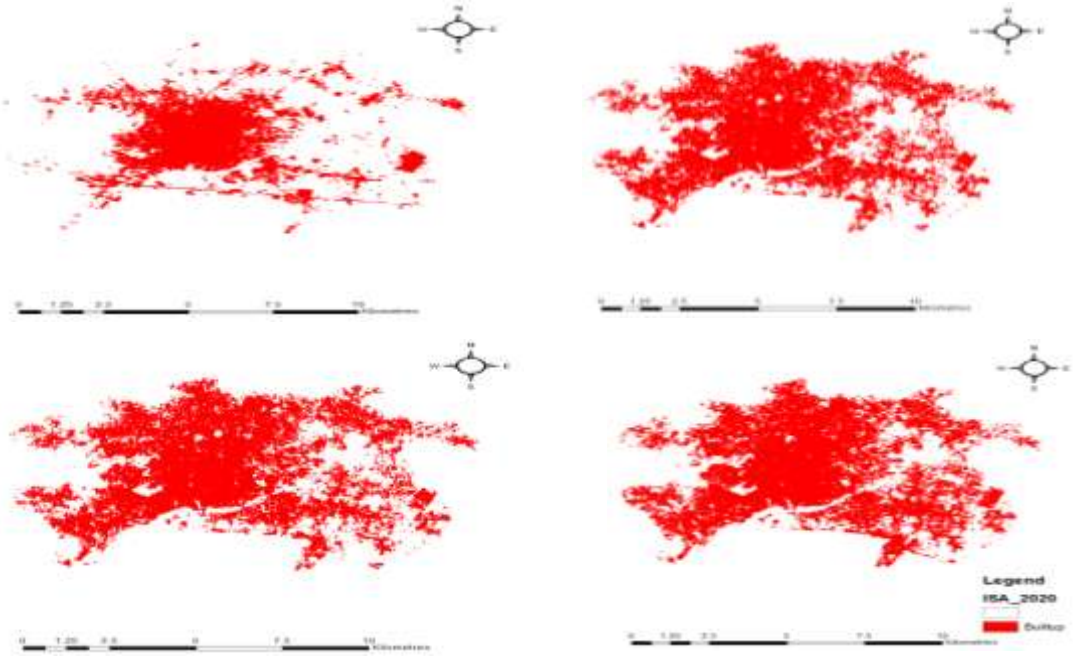

Fig. 6: ISA / built-up area maps of Ijebu-ode on December 18 2005, January 01 2010, January 06 2015 and January 04 2020

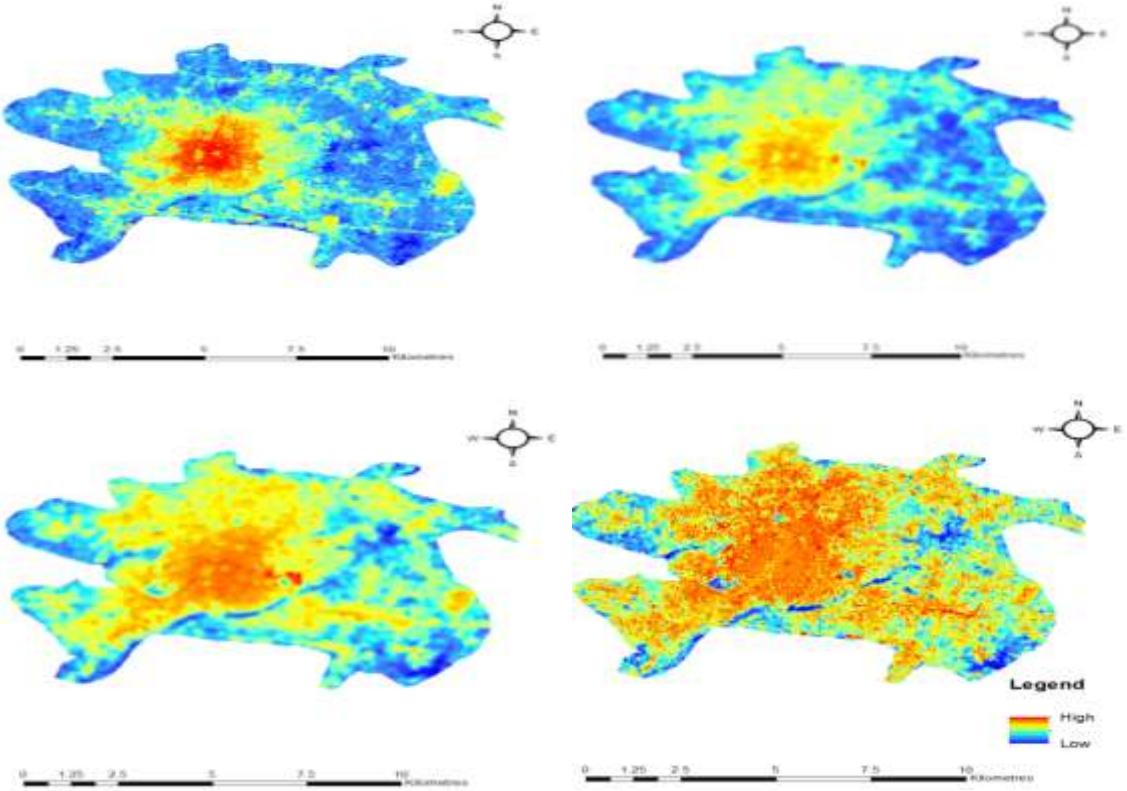

Fig. 7: Spatiotemporal patterns of land surface temperature (LST) in Ijebu-ode city on December 18 2005, January 01 2010, January 06 2015 and January 04 2020

Discussion

It has been stated that land cover is the observed physical features on the Earth's surface that changes into a land use when an economic function is added to it (Singh, 2016). The rapid pace of urbanization has resulted in an increase in city size, which has resulted in significant changes in LULC (Li *et al*., 2017; Khandelwal *et al*., 2018; Adedeji *et al*., 2020; Imran and Mehmood, 2020; Aigbokhan *et al*., 2023). Urbanization has allowed Ijebu-ode to sprawl freely, particularly in the surrounding rural areas, culminating in its gradual encroachment on vast forested areas and farm land, posing climatic and hydrogeological risks, such as flooding and erosion (Neog, 2021). As the city's population has grown over time, it has seen unprecedented growth in ISA in the form of residential, commercial, industrial, transportation network, and parking lots (Alkaradaghi *et al*., 2019), which influences the city's local climate (Estoque *et al*., 2017; He *et al*., 2020; Yin *et al*., 2022). In 2005, Ijebu-ode had high vegetation densities in the surrounding areas, with NDVI value of 0.266, in contrast to the city's central region, which had a low vegetation density class index of -0.102. Higher NDVI values typically indicate a greater fraction of vegetation in a pixel, and studies have shown that as vegetation increases, so do NDVI values (Huang *et al*., 2021; Farid *et al*., 2022). The areas with the most forest had the highest mean NDVI, whereas the areas with the least vegetation, particularly in the central parts, had the lowest mean NDVI. More of the city was dominated by sparse vegetation density in 2020, with values of 0.048 and 0.357. This demonstrates how vegetation density changes between 2005 and 2020 as a result of the area's reduction in vegetation due to built-up (Huang *et al*., 2021). The NDBI results showed gradual increase in built-up areas and high LST. In addition, Table 4 shows the land cover categories in terms of built-up and non-built-up and it revealed that the built-up significanstly increased by 150.25 % while the non-built-up correspondingly decreased by -56.77 % during the period of study. This also indicated that built-up areas or urbanization create much more surface temperature variations. Kasim *et al*. (2020) corroborated this in a study of land use, land cover change, and land surface emissivity in Ibadan, Nigeria. Several studies have found that high temperature anomalies are closely associated with built-up land, densely populated zones, and heavily industrialised areas (Zheng *et al*., 2021). Between 2005 and 2020, there has been a noticeable increase in the number of ISAs, which is likely to influence the local climate. The expansion of impervious surfaces as a result of urban expansion will raise the LST, potentially causing uneven distribution of urban heat (Zheng *et al*., 2021). According to Yuan and Bauer (2007), LST measurements typically represent the radiometric temperatures of vegetated and non-vegetated surfaces, primarily impervious surfaces, in the study site's urbanized area where bare soil is limited. It can be seen that changes in the LST over time correspond to rapid changes in land use/land cover. Due to rapid urban expansion and population growth during the study period, the changing LULC dynamics have a significant impact on the distribution of the LST (Sun *et al*., 2012; Li *et al*., 2015; Choudhury *et al*. 2019; Yin *et al*., 2022). In a similar study in Lahore, Pakistan, Farid *et al*. (2022) discovered that urbanization has influenced LST, and that maximum LST consistently increased with increase in built-up land. It is undeniable that deforestation caused by rapid urbanization has contributed to increased LST and greenhouse gas emissions, thereby impacting climate change (Choudhury *et al*. 2019; Yin *et al*., 2022).

Table 4: Land cover categories in terms of built-up and non-built-up in Ijebu-ode (2005-2020)

Land cover categories	Land cover area (Ha)				Growth Rate (%)
	2005	2010	2015	2020	2005-2020
Built-up	2374.3	3088.35	4758.65	5941.62	150.25
Non-built-up	6277.61	5568.55	3898.46	2713.94	-56.77

Mukherjee and Singh (2020) found a negative correlation between the NDVI and LST in cities with increasing temperatures of 2.13°C per decade in their study of spatial and temporal changes in land use and vegetation patterns and their impact on LST in two Indian cities. LST is determined by the latent heat flux from the surface to the atmosphere via evapotranspiration, and lower LSTs are mostly found in areas with high NDVI (Yuan and Bauer, 2007; Mukherjee and Singh, 2020; Farid *et al*., 2022). The unprecedented urban development and population growth in Ijebu-ode city have resulted in the replacement of natural land surfaces by ISAs such as asphalt roads, residential and industrial buildings, and other forms of construction, causing major land use changes that have contributed to the rise in urban temperature (Rasul *et al*., 2017; Mukherjee and Singh, 2020; Imran *et al*., 2021; Yang *et al*., 2020; Zhang *et al*., 2022).

Buildings and paved surfaces in urban areas also tend to cause greater infrared radiation retention and delayed heat release (Orimoloye *et al*., 2018; Mukherjee and Singh, 2020). Furthermore, Rasul *et al*. (2017) discovered that asphalt parking lots have their own microclimate due to their low thermal conductivity and albedo. Building density has also been identified as a significant influence of LST (Li *et al*., 2017). The built-up areas (primarily commercial and residential) in the study area were found to have high LST due to very low vegetation cover and the fact that radiations are trapped by the various building and construction materials used. This is supported by previous research findings (Zhang *et al*., 2017; Yang *et al*., 2020; Imran *et al*., 2021). LST has frequently been discovered to be closely related to the percentage of ISA in urban areas (Yuan and Bauer, 2007; Yang *et al*., 2020). Guo *et al*. (2019) reported an 8% increase in ISAs from 2005 to 2015 in Beijing, China, resulting in an ISA mean LST of about 2°C. Low LST is observed in all study periods in the study area's periphery due to the abundance of vegetal cover, which helps to trap moisture (Estoque *et al*., 2017; Liu *et al*., 2022). Furthermore, vegetation lowers surface temperatures by providing a shading layer that protects land surfaces from direct sunlight (Estoque *et al*., 2017; Lu *et al*., 2020; Liu *et al*., 2022).

Conclusions

The effect of population density and land use land cover changes on the development of land surface temperature (LST) in Ijebu-ode, Nigeria, was studied for the years 2005, 2010, 2015, and 2020. The study's findings revealed that significant changes in land use/land cover patterns occurred in the study area between 2005 and 2020. Vegetation (forest/farmland) was the dominant land cover in 2005, accounting for approximately 5557 hectares (64.23%), but it was mostly converted to urban built-up areas by 2020. In general, urban built area expanded at the expense of non-built-up land, indicating urban expansion caused by population growth. The spatial metrics results revealed that the extracted NDVI values were higher in semi-urban/rural areas during the study periods. The thermal environment, including land surface temperature, changes as urban populations grow and urban built-up areas expand. From 2005 to 2020, the study area saw an increase in the spatial distribution of LST, particularly in the city centre and spreading to surrounding areas where urban expansions are emerging. The surface temperature of Ijebu-ode City ranged from mean of 22.17 °C in 2005 to 26.62 °C in 2020 showing an increase of 4.60 ºC. The spatial distribution of LST in the study area clearly showed that built-up areas and baregrounds exhibited higher LST than vegetation due to their low thermal inertia and transpiration. This implied that vegetation cover reduces the Land Surface Temperature (LST) over the land surface; therefore, vegetative surfaces like urban parks, home gardens, and forest reserves should be promoted and preserved in the city.

Acknowledgements

The authors wish to acknowledge the constructive and clear remarks made by the anonymous people that read this article before final submission and sincere gratitude goes to all the collaborating scientists.

Reference

Adedeji, O.H., Adeofun, C.O., Tope-Ajayi, O.O. and Ogunkola, M.O. (2020). Spatio-temporal analysis of urban sprawl and land use / land cover changes in a suburb of Lagos and Ogun metropolises, Nigeria (1986-2014). *Ife Journal of Science*. 22(1):1-16.

Aigbokhan, O.J., Adedeji, O.H., Oladoye, A.O. and Oyedepo, J.A. (2023). Dynamics of urban landscape and its thermal interactions with selected land cover types: a case of Benin City, Nigeria. *Journal of Applied Life Sciences and Environment*. 56 (2), 245-272.

Alkaradaghi, K., Ali, S.S., Al-Ansari, N. and Laue, J. (2019). Land Use Classification and Change Detection Using Multi-temporal Landsat Imagery in Sulaimaniyah Governorate, Iraq. 117-120, In: H. M. El-Askary *et al*. (eds.), Advances in Remote Sensing and Geo Informatics Applications, Advances in Science, Technology & Innovation. https://doi.org/10.1007/978-3-030-01440-7_28 (Accessed 14 September 2022).

Chen, W., Zhang, Y., Pengwang. C. and Gao, W. (2017). Evaluation of Urbanization Dynamics and its Impacts on Surface Heat Islands: A Case Study of Beijing, China. *Remote Sens.*, 9, 453.

Chen, Y., Yang, J., Yang, R., Xiao, X. and Xia, J.C. (2022). Contribution of urban functional zones to the spatial distribution of urban thermal environment. *Build. Environ*. 216, 109000.

Choudhury, D., Das, K. and Das, A. (2019). Assessment of land use land cover changes and its impact on variations of land surface temperature in Asansol-Durgapur development region. *Egypt J Remote Sens Space Sci.* 22(2):203–218.

Dijkstra, L., Poelman, H. and Veneri, P. (2019). The EU-OECD definition of a functional urban area. In *OECD Regional Development Working Papers*; OECD: Paris, France, p.11. Available online: https://www.oecd-ilibrary.org/urban-rural-and-regionaldevelopment/the-eu-oecd-definition-of-a-functional-urban-area_d58cb 34d-en (Accessed 14 July 2022)

Estoque, R.C., Murayama, Y. and Myint, S.W. (2017). Effects of landscape composition and pattern on land surface temperature: an urban heat island study in the megacities of Southeast Asia. *Science of the Total Environment*. 577: 349–359.

Farid, N., Moazzam, M.F.U., Ahmad, S.R., Coluzzi, R. and Lanfredi, M. (2022). Monitoring the Impact of Rapid Urbanization on Land Surface Temperature and Assessment of Surface Urban Heat Island Using Landsat in Megacity (Lahore) of Pakistan. *Front. Remote Sens.* 3:897397.

Guo, L., Liu, R., Men, C., Wang, Q., Miao, Y. and Zhang, Y. (2019). Quantifying and Simulating Landscape Composition and Pattern Impacts on Land Surface Temperature: A Decadal Study of the Rapidly Urbanizing City of Beijing, China. *Science of the Total Environment*. 654, 430–440.

He, B.J., Wang, J., Liu, H. and Ulpiani, G. (2020). Localized synergies between heat waves and urban heat islands: Implications on human thermal comfort and urban heat management. *Environmental Research*. 193. 110584.

Huang, S., Tang, L., Hupy, J.P., Wang, Y. and Shao, G. (2021). A commentary review on the use of normalized difference vegetation index (NDVI) in the era of popular remote sensing. *J. For. Res.*, 32(1):1–6

Imran, M. and Mehmood, A. (2020). Analysis and Mapping of Present and Future Drivers of Local Urban Climate Using Remote Sensing: a Case of Lahore, Pakistan. *Arabian J. Geosciences*, 13: 1–14.

Imran, H.M., Hossain, A., Saiful Islam, A.K.M., Rahman, A., Bhuiyan, M.A.E., Paul, S. and Alam, A. (2021). Impact of Land Cover Changes on Land Surface Temperature and Human Thermal Comfort in Dhaka City of Bangladesh. *Earth Systems and Environment*, 5:667–693

Jensen, J.R. (2009). Remote Sensing of the Environment: An Earth Resource Perspective, Pearson Education India, Bengaluru, India.

Kasim, O., Agbola, S. and Oweniwe, M. (2020). Land use land cover change and land surface emissivity in Ibadan, Nigeria. *Town and Regional Planning*, 77: 71-88.

Khandelwal, S., Goyal, R., Kaul, N. and Mathew, A. (2018). Assessment of land surface temperature variation due to change in elevation of area surrounding Jaipur, India. *The Egyptian Journal of Remote Sensing and Space Sciences*, 21: 87–94.

Li, Z.L., Wu, H., Wang, N., Qiu, S., Sobrino, J.A., Wan, Z., Tang, B. and Yan, G. (2013). Land surface emissivity retrieval from satellite data.

International Journal of Remote Sensing, 34: 3084 – 3127.

Li, D., Sun, T., Liu, M., Yang, L., Wang, L. and Gao, Z. (2015). Contrasting responses of urban and rural surface energy budgets to heat waves explain synergies between urban heat islands and heat waves. *Environ. Res. Lett.*, 10, 1–10.

Li, X., Kamarianakis, Y., Ouyang, Y., Turner, B.L. and Brazel, A. (2017). On the association between land system architecture and land surface temperatures: Evidence from a Desert Metropolis—Phoenix, Arizona, U.S.A. *Landsc. Urban Plan*. 163, 107–120.

Li, W., Han, C., Li, W., Zhou, W. and Han, L. (2020). Multi-scale effects of urban agglomeration on thermal environment: A case of the Yangtze River Delta Mega region, China. *Science of the Total Environment.* 713, 136556.

Liu, J., Jiao, L., Zhang, B., Xu, G., Yang, L., Dong, T., Xu, Z., Zhong, J. and Zhou, Z. (2021). New indices to capture the evolution characteristics of urban expansion structure and form. *Ecological Indicators*. 122: 107302.

Liu, S., Li, X.; Chen, L., Zhao, Q., Zhao, C., Hu, X. and Li, J. (2022). A New Approach to Investigate the Spatially Heterogeneous in the Cooling Effects of Landscape Pattern. *Land*, 11: 239.

Loranty, M., Davydov, S., Kropp, H., Alexander, H., Mack, M., Natali, S. and Zimov, N. (2018). Vegetation indices do not capture forest cover variation in Upland Siberian larch forests. *Remote Sens*ing. 10(11):1686 – 1700.

Lu, L., Weng, Q., Xiao, D., Guo, H., Li, Q. and Hui, H. (2020). Spatiotemporal Variation of Surface Urban Heat Islands in Relation to Land Cover Composition and Configuration: A Multi-Scale Case Study of Xi'an, China. *Remote Sensing*, 12(17): 2713

Mukherjee, F. and Singh, D. (2020). Assessing Land Use-Land Cover Change and Its Impact on Land Surface Temperature Using LANDSAT Data: A Comparison of Two Urban Areas in India. *Earth Systems and Environment*. 4:385-407.

Neog, R. (2021). Evaluation of temporal dynamics of land use and land surface temperature (LST) in Agartala city of India. *Environment, Development and Sustainability*, 24: 3419–3438.

National Population Commission (NPC). 2006. https://nationalpopulation.gov.ng/census-enumeration (Accessed 14 July 2022).

Nkwunonwo, U.C., Tobore, A. and Nwaka, O.C. (2023). Ecosystem-based approach to local flood risk management in Ogun State, Nigeria: Knowledge, and pathway to Actualisation, *Natural Hazard Research*, 4(3): 357–373.

Ogunjobi, K.O., Adamu, Y., Akinsanola, A.A. and Orimoloye, I.R. (2018). Spatiotemporal analysis of land use dynamics and its potential indications on land surface temperature in Sokoto Metropolis, Nigeria. *R. Soc. Open Sci*. 5, 180661. http://dx.doi.org/10.1098/rsos.180661 (Accessed 19 November 2022).

Oke, T.R. (1987). Boundary Layer Climates (2nd Ed.). Methuen and Co.pp. 262–303.

Orimoloye, I.R., Mazinyo, S.P., Nel, W. and Kalumba, A.M. (2018). Spatiotemporal monitoring of land surface temperature and estimated radiation using remote sensing: human health implications for East London, South Africa. *Environment and Earth Science*, 77(3): 1 – 10.

Population HUB (2022). World Population 2022: Earth Population - Statistics. https://population-hub.com/en/population-of-earth.html (Accessed 14 July 2022).

Qin, Z., Karnieli, A. and Berliner, P. (2001). A mono-window algorithm for retrieving land surface temperature from Landsat TM data and its application to the Israel-Egypt border region. *International Journal of Remote Sensing*, 22:3719–3746.

Ranagalage, M., Estoque, R.C., Handayani, H.H., Zhang, X., Morimoto, T., Tadono, T. and Murayama, Y. (2018). Relation between Urban Volume and Land Surface Temperature: A Comparative Study of Planned and Traditional Cities in Japan, *Sustainability*, 10: 2366;

Rasul, A., Balzter, H. and Smith, C. (2017). Applying a normalized ratio scale technique to assess

influences of urban expansion on land surface temperature of the semi-arid city of Erbil. *International Journal of Remote Sensing*, 38(13): 3960-3980.

Singh, S.K. (2016). Geospatial Technique for Land use/Land cover mapping using Multi- Temporal Satellite Images: A case study of Samastipur District (India). *Environment & We: An International Journal of Science and Technology*, 11(2-4): 75-85.

Sobrino, J.A., Jiménez-Munõz, J.C., Sòria, G., Romaguera, M., Guanter, L., Moreno, J. and Martínez, P. (2008). Land surface emissivity retrieval from different VNIR and TIR sensors. *IEEE Transactions on Geoscience and Remote Sensing*, 46(2): 316–327.

Sun, Q., Wu, Z. and Tan, J. (2012). The relationship between land surface temperature and land use/land cover in Guangzhou, China. *Environment and Earth Science*, 65: 1687–1694

Tiwari, P.C. and Joshi, B. (2015). Climate change and rural outmigration in Himalaya. *The Journal of Change and Adaptation in Socio-Ecological Systems (CASES)*, 2: 8–25

Tobore, A.O., Nkwunonwo U.C. and Senjobi, B. (2024). Combined remote sensing and multi-criteria analysis of wetland soil potential for rice production: case study of Ogun River basin, Nigeria, *African Geographical Review*, 10.1080/19376812.2022.2104736.

United Nations. Department of Economic and Social Affairs, Population Division. (2018). World Urbanization Prospects: The 2018 Revision (ST/ESA/SER.A/420). United Nations, New York Available at https://population.un.org/wup /Publications/Files/WUP2018-Report.pdf. 2018. (Accessed 14 July 2022).

USGS (2016). Landsat 8 Data Users Handbook, USGS, Reston, VA, USA.

Voogt, J.A. and Oke, T.R. (2003). Thermal remote sensing of urban climates. *Remote Sensing of Environment*, 86: 370–384.

Wu, Y., Li, S. and Yu, S. (2016). Monitoring urban expansion and its effects on land use and land cover changes in Guangzhou city, China. *Environmental Monitoring and Assessment*, 188:54

Yang, H., Xi, C., Zhao, X., Mao, P., Wang, Z., Shi, Y., He, T. and Li, Z. (2020). Measuring the Urban Land Surface Temperature Variations under Zhengzhou City Expansion Using Landsat-Like Data. *Remote Sensing*, 12: 801.

Yin, S., Liu, J. and Han, Z. (2022). Relationship between urban morphology and land surface temperature—A case study of Nanjing City. *PLoS ONE*, 17(2): e0260205.

Yuan, F. and Bauer, M.E. (2007). Comparison of impervious surface area and normalized difference vegetation index as indicators of surface urban heat island effects in Landsat imagery. *Remote Sensing of Environment*, 106(3): 375-386.

Zha, Y., Gao, J. and Ni, S. (2003). Use of normalized difference built-up index in automatically mapping urban areas from TM imagery. *International Journal of Remote Sensing*, 24: 583–594

Zhang, Y., Zhang, C., Yang, K., Peng, Z., Tang, L., Duan, H., Wu, C. and Luo, Y. (2022). Temporal and Spatial Effects of Urbanization on Regional Thermal Comfort. *Land*, 11: 688.

Zheng, Y., Tang, L. and Wang, H. (2021). An improved approach for monitoring urban built-up areas by combining NPP-VIIRS nighttime light, NDVI, NDWI, and NDBI. *Journal of Cleaner Production*, 328: 129488